

${}^6\text{Li}(n, d){}^5\text{He}$ and ${}^7\text{Li}(n, d){}^6\text{He}$ with 56.3 MeV neutrons*

F. P. Brady, N. S. P. King,[†] B. E. Bonner,[†] M. W. McNaughton,[†] and J. C. Wang[§]
Crocker Nuclear Laboratory and Department of Physics, University of California, Davis, California 95616

William W. True

Department of Physics, University of California, Davis, California 95616

(Received 29 March 1977)

The angular distributions of deuterons for $7^\circ \leq \theta_{\text{c.m.}} \leq 60^\circ$ have been measured for 56.3 MeV neutrons incident on targets of ${}^6\text{Li}$ and ${}^7\text{Li}$. Transitions corresponding to the pickup of $1p$ -shell and $1s$ -shell protons are strong with the latter exhibiting structure indicative of groups of excited states in ${}^5\text{He}$ and ${}^6\text{He}$. In ${}^5\text{He}$ these have excitation energies of 16.7, 18.5, and 20.5 MeV, and in ${}^6\text{He}$ an average excitation energy of 15.6 MeV. The spectroscopic factors deduced from the measurements are in good agreement with theoretical values where the latter are available.

[NUCLEAR REACTIONS ${}^6\text{Li}(n, d)$, ${}^7\text{Li}(n, d)$; 56.3 MeV neutrons, measured $\sigma(\theta)$, deduced spectroscopic factors.]

I. INTRODUCTION

There have been a number of papers describing the results of (p, d) reactions on ${}^6\text{Li}$ and ${}^7\text{Li}$ at incident proton energies high enough to assure that the reaction mechanism is predominantly direct. In particular, data and analyses exist at proton energies of 33.6,¹ 100,^{2,3} and 156 MeV.⁴ Earlier these reactions were studied at 18,⁵⁻⁷ 39.8,⁸ and 95 MeV.⁹

The (n, d) angular distributions to the ground states of ${}^5\text{He}$ and ${}^6\text{He}$ have been measured with 14.4 MeV neutrons incident on ${}^6\text{Li}$ ¹⁰ and ${}^7\text{Li}$.^{11,12} With a 152 MeV neutron beam of modest resolution (≈ 6 MeV) incident on ${}^6\text{Li}$, broad structures are interpreted as transitions to the ground state of ${}^5\text{He}$ and to a state near 14 MeV excitation in ${}^5\text{He}$ corresponding respectively to proton pickup from the $1p$ and $1s$ shells.¹³ Similar results are found in the case of a ${}^7\text{Li}$ target.¹³

Proton-induced reactions in general and (p, d) reactions in particular have provided much valuable information on nuclear structure. However, there exist few data on neutron-induced reactions which have been useful from a spectroscopic standpoint. At medium and intermediate energies (≥ 50 MeV), neutron-induced reactions have in the past suffered from various deficiencies including poor neutron beam intensity and energy resolution, low angular and energy resolution of the charged-particle detection system and inadequate determination of the absolute cross sections. We have made improvements which reduce the above deficiencies while using neutron energies (≥ 25 MeV) which should assure that direct reaction mechanisms dominate.

In this paper, experimental results and distorted-wave-Born-approximation (DWBA) analyses are reported for (n, d) reactions on ${}^6\text{Li}$ and ${}^7\text{Li}$ nuclei produced by a beam of 56.3 MeV neutrons with energy resolution [full width at half maximum (FWHM)] of ≈ 1 MeV. Angular distributions from 7° to 60° lab were measured. In addition to transitions to the ground state and 16.7 MeV state of ${}^5\text{He}$ there is evidence for states near 18.5 and 20.5 MeV. In the case of ${}^7\text{Li}(n, d){}^6\text{He}$ transitions to the ground and first excited (1.8 MeV) states are observed and transitions to what appears to be a group of states between about 13 and 18 MeV excitation in ${}^6\text{He}$. Spectroscopic factors are extracted and compared with theoretical predictions where available.

II. EXPERIMENTAL METHOD

Protons from the isochronous cyclotron at Crocker Nuclear Laboratory were used to produce the neutron beam via the ${}^7\text{Li}(p, n)$ reaction. In the present case the proton beam bursts arrive at the ${}^7\text{Li}$ target about every 50 ns and have a time width (FWHM) of ≈ 1.4 ns.

The original unpolarized neutron beam facility¹⁴ has been modified to allow incorporation of a scattering chamber for charged-particle detection. Details of the facility, the data capture, and both on-line and off-line data analyses procedures are described in Ref. 15.

The neutrons are collimated to form a beam of cross sectional size 12 mm wide by 24 mm high, and of intensity $\approx 10^6$ n/s in the well defined peak of 1 MeV FWHM. Figure 1 shows the overall arrangement for beam production, charged-particle

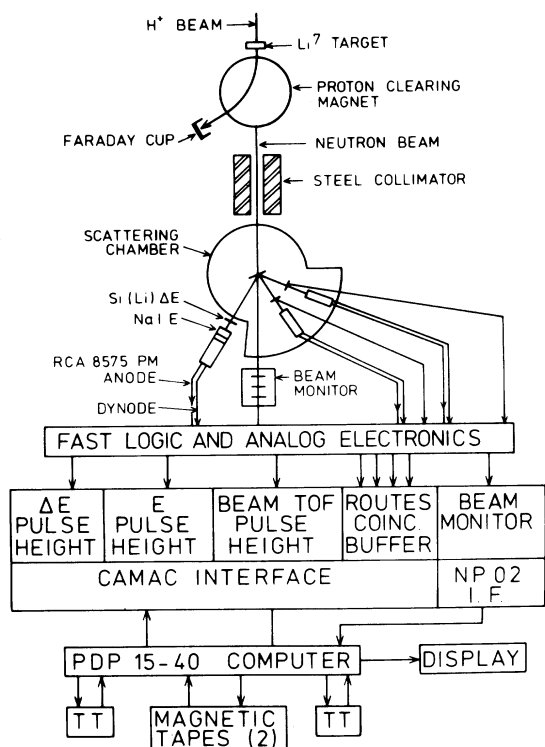


FIG. 1. Schematic of the experimental arrangement for neutron beam production, charged particle detection, and data capture.

detection, and data capture. The beam passes through the collimator into the scattering chamber, all in vacuum, and its intensity is monitored by a high-stability recoil-proton telescope behind the chamber. Integration of the proton beam cleared into a Faraday cup provides a secondary neutron beam monitor accurate to 1–2%. The target in the scattering chamber is 3 m from the ${}^7\text{Li}$ target. Each of the three ΔE - E telescopes, two mounted in the scattering chamber and one outside, consists of a solid state detector and a NaI scintillator coupled to an RCA 8578 phototube. Zero-crossing timing signals relative to a beam pickoff reference mounted just upstream of the ${}^7\text{Li}$ target are used to select the beam peak by a time of flight (TOF) method. Analog data, in addition to a detector identification signal, are transferred to an on-line PDP 15/40 computer via a Camac interface, and recorded, event by event on standard magnetic tape.

Data were taken with a neutron beam of ≈ 900 keV FWHM and an average overall system resolution of ≈ 1.6 MeV owing to detector resolution, finite solid angle, and target thickness. The lithium targets were made from $>99\%$ isotopic purity lithium metal, cleaved under oil, and pressed into a thin self-supporting target on a frame. The ${}^6\text{Li}$

target was 19.9 mg/cm^2 and the ${}^7\text{Li}$ was 33.4 mg/cm^2 . In some cases a very thin layer of acrylic was sprayed on the target as a protection against the effects of air and water vapor during transportation to and pump down in the scattering chamber.¹⁶ Helium bags were also used during pressing and transport.

III. DATA ANALYSIS AND RESULTS

Both on-line and off-line data analyses were carried out. The usual method of sorting the event-by-event data is to first select the particle type (proton, deuteron, etc.) by making cuts on the two-parameter ΔE vs E spectra. (Sometimes a rough TOF cut is made first.) Then the two-parameter TOF vs E spectra are displayed for the events corresponding to the particle of interest, and cuts are made to select the events associated with the neutron beam peak. This time cut will also include events due to a small range (~ 1 MeV) of lower beam energies (≤ 14 MeV) due to earlier proton and neutron beam bursts. However, these events are at lower energies than those of interest here.

Figures 2 and 3 show histograms of events from ${}^6\text{Li}(n, d){}^5\text{He}$ and ${}^7\text{Li}(n, d){}^6\text{He}$ after particle type and time restrictions have been made. The background of events with target removed is small for the lowest states and about 15% of the continuum under the excited states which are believed to be due to proton pickup from the $1s_{1/2}$ shell.

Peak strengths were extracted using Gaussian fitting. For the (unbound) ground state of ${}^5\text{He}$ the situation is complicated by the possibility of contamination by the (presumably broad) $1p_{1/2}$ state of ${}^5\text{He}$. Also the $1p_{3/2}$ ground state peak of ${}^5\text{He}$ is asymmetric with the tail manifesting the effects of the $n + {}^4\text{He}$ final state interaction. In the case of ${}^7\text{Li}(n, d){}^6\text{He}$ to the ground and first excited states there is also a continuum beginning at 0.97 MeV excitation in ${}^6\text{He}$. The dashed lines in Figs. 2 and 3 show schematically the assumed backgrounds.

The energy spectra in Figs. 2 and 3 show evidence for peaks between about 16 and 21 MeV excitation in ${}^5\text{He}$ and between about 13 and 18 MeV in ${}^6\text{He}$. The state at 16.76 MeV in ${}^5\text{He}$ is well established, in a number of experiments, as having $J^\pi = \frac{3}{2}^+$ and $\Gamma \approx 135$ keV (lab).¹⁷ There is also evidence for a number of broad overlapping states including a state or a group of states at 19.9 ± 0.4 MeV excitation with $\Gamma \approx 3$ MeV.¹⁷ Sequential reactions¹⁸ initiated via $\alpha + d$ at $E_\alpha = 70$ MeV through ${}^5\text{He}$ excited states produced results suggestive of narrow ($\Gamma \approx 180$ keV) structures at 18.6, 18.8, and 19.2 MeV excitation in ${}^5\text{He}$. The less preferred interpretation¹⁸ is that of broad

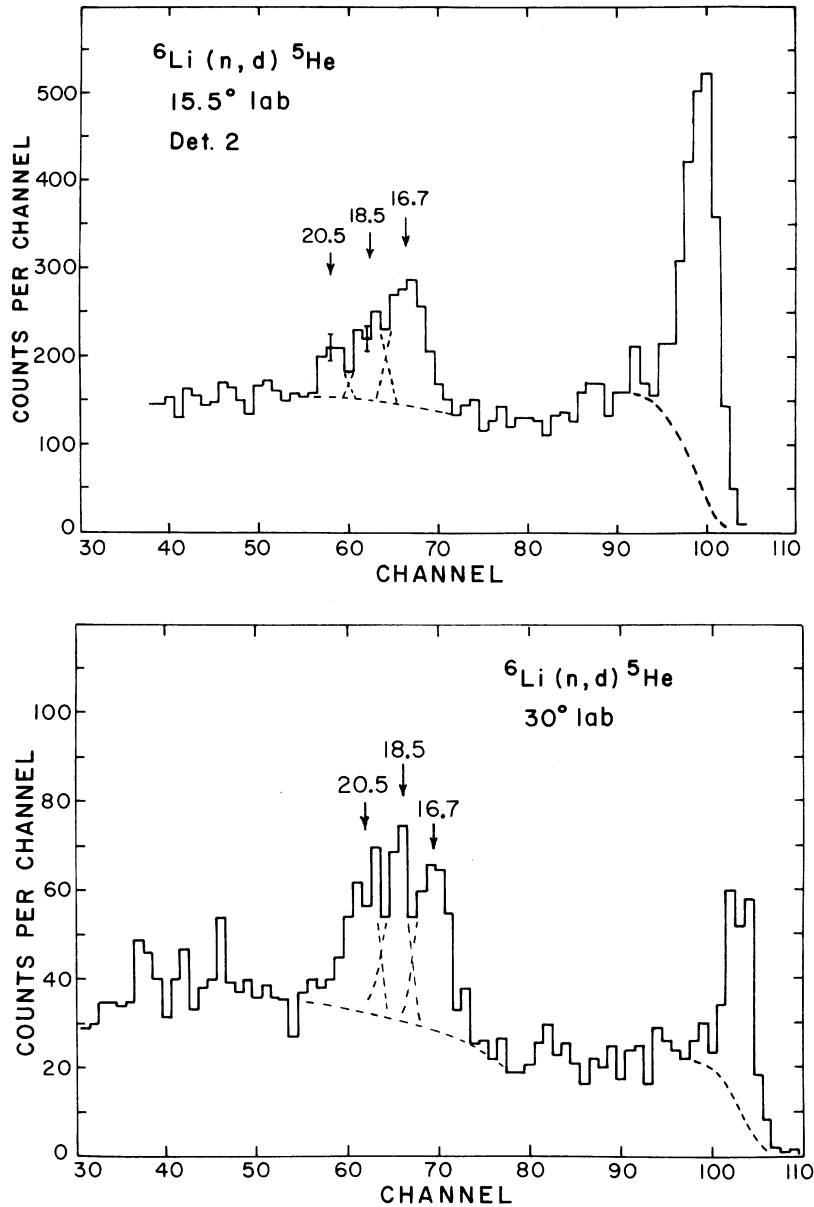


FIG. 2. Histograms of ${}^6\text{Li}(n,d){}^5\text{He}$ data at two angles from different detector telescopes.

($\Gamma \approx 1.6$ MeV) structures centered at 18.7 and 19.0 MeV. In ${}^5\text{Li}$ there is the $J^\pi = \frac{3}{2}^+$ analog at 16.66 MeV ($\Gamma \approx 450$ keV) and evidence for broad states centered at 18 ± 1 MeV and 20 ± 0.5 MeV excitation. (See Ref. 17 and references therein.)

The energy spectra from ${}^6\text{Li}(n,d){}^5\text{He}$ show evidence for peaks at 16.7, 18.5, and 20.5 MeV. The energy positions of these vary with angle as expected kinematically and the spectra from different angles appropriately shifted and summed show the peaks as well. However, the energy resolution of the system and/or the finite width of the peaks

plus the limited statistics make the presence of these states at 18.5 ± 0.5 and 20 ± 0.5 MeV not completely certain. In addition, one cannot rule out additional weaker and/or broader states also being present. On the basis of the present data and the evidence from other experiments as discussed above, the data were analyzed assuming only these three excited states are present and that their widths are less than the system resolution. A smooth "background" drawn arbitrarily as shown by the dashed lines in Fig. 2 was subtracted out first.

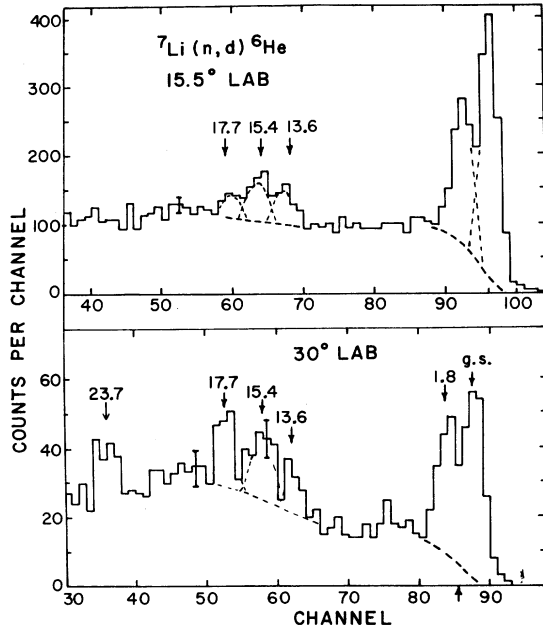


FIG. 3. Histograms of ${}^7\text{Li}(n,d){}^6\text{He}$ data at two angles from different detector telescopes.

In the case of ${}^6\text{He}$ populated here via ${}^7\text{Li}(n,d){}^6\text{He}$, evidence for states at 13.4 ± 0.5 ($\Gamma \approx 1.2$ MeV) and at 15.3 ± 0.3 MeV has been presented.^{19,20} The evidence for the 13.4 MeV state comes mainly from ${}^7\text{Li}(p,2p){}^6\text{He}$ at 156 MeV,¹⁹ while the evidence for the 15.3 MeV state comes from Ref. 19 and from ${}^6\text{Li}(\pi^-, \gamma){}^6\text{He}$ measurements.²⁰ However, more recent and improved $(p,2p)$ data,²¹ while showing a broad structure with possible internal structure extending from ≈ 13 to 18 MeV excitation, do not resolve states at 13.4 and 15.3 MeV nor do 80 MeV ${}^7\text{Li}(d, {}^3\text{He}){}^6\text{He}$ data²² with 200 keV resolution show this doublet structure.

In the present ${}^7\text{Li}(n,d){}^6\text{He}$ data there does appear to be some structure extending from about 13 to 18 MeV excitation. In particular there is possible evidence for states near 13.6, 15.4, and 17.7 MeV (± 0.5 MeV) excitation. However, the structure pattern was not always consistent from angle to angle and identification of individual states is made difficult by the limited statistics obtained during nearly 100 h of beam. As in the case of ${}^5\text{He}$, one cannot rule out the presence of other weaker or broader states. Therefore in the data analysis the states in the structure from 13 to 18 MeV excitation were combined so that the whole structure was integrated above an arbitrary "smooth" background such as that shown by the dashed lines in Fig. 3. The average excitation was taken to be 15.6 MeV. There is evidence, Fig. 3, for structure near 23.7 MeV excitation and its appearance

TABLE I. Cross sections and uncertainties for ${}^6\text{Li}(n,d){}^5\text{He}$ in mb/sr.

$\theta_{c.m.}$	$\sigma_{c.m.}$	$\Delta\sigma_{c.m.}$
d_0 (g.s.)		
6.37	12.01	1.40
12.7	7.19	0.70
19.7	4.63	0.41
25.4	2.28	0.42
31.6	1.62	0.21
37.9	1.25	0.22
50.1	0.554	0.07
56.2	0.393	0.07
62.1	0.167	0.05
73.7	0.107	0.04
d_1 (16.7 MeV)		
6.72	5.62	1.05
13.4	2.23	0.30
20.8	0.717	0.070
26.8	0.326	0.100
33.4	0.473	0.070
39.9	0.395	0.050
52.8	0.128	0.040
59.1	0.101	0.040
66.2	0.045	0.030
77.3	0.024	0.014
d_2 (18.5 MeV)		
6.8	2.4	0.06
13.5	0.9	0.19
20.9	0.36	0.10
27.0	0.405	0.104
33.6	0.359	0.058
40.2	0.372	0.07
53.2	0.363	0.08
59.5	0.181	0.044
65.8	0.120	0.034
77.9	0.040	0.020
d_3 (20.5 MeV)		
6.8	1.02	0.20
13.6	0.565	0.14
21.7	0.232	0.04
27.2	0.183	0.07
33.9	0.224	0.05
40.5	0.38	0.08
53.6	0.257	0.08
60.0	0.221	0.05
66.2	0.171	0.07
78.4	0.051	0.03

above the continuum at 30° but it is not so clear at more forward angles and suggests a transfer of $l \geq 2$. From ${}^6\text{Li}(\pi^-, \gamma){}^6\text{He}$ measurements,²⁰ a broad structure is reported at 23.2 ± 0.7 MeV.

The absolute cross sections were obtained by normalizing to the $n-p$ differential cross sections which are known to about 2.5% near this energy²³ and can be extrapolated using phase shift fits.²⁴ The absolute normalization is estimated to have an

TABLE II. Cross sections for ${}^7\text{Li}(n,d){}^6\text{He}$ in mb/sr.

$\theta_{c.m.}$	$\sigma_{c.m.}$	$\Delta\sigma_{c.m.}$
d_0 (g.s.)		
6.2	4.7	0.6
8.7	5.03	0.50
12.4	4.92	0.5
18.6	3.24	0.37
19.2	2.76	0.32
24.8	2.05	0.2
31.0	1.36	0.15
33.3	1.08	0.15
37.0	1.07	0.12
43.1	0.736	0.08
49.1	0.557	0.07
55.0	0.32	0.06
60.1	0.33	0.07
66.6	0.147	0.055
d_1 (1.8 MeV)		
6.25	3.25	0.8
8.7	3.6	0.40
12.5	2.50	0.25
18.7	2.17	0.2
19.3	1.68	0.17
24.9	1.70	0.17
31.1	0.95	0.1
33.3	1.10	0.1
37.2	0.907	0.1
43.3	0.899	0.1
49.3	0.68	0.07
55.2	0.31	0.06
60.8	0.33	0.07
66.8	0.153	0.05
$d_2 + d_3 + d_4$ (15.6 MeV)		
6.5	3.44	1.2
9.0	4.38	1.0
13.1	2.04	0.5
19.6	1.4	0.5
32.5	0.71	0.11
38.8	0.90	0.12
45.2	0.52	0.11

uncertainty of 10% due mainly to uncertainties in the lithium target thicknesses and uniformities.

The uncertainties quoted in Tables I and II and shown in the plots of Figs. 4–6 do not include this normalization error. They do include statistical uncertainties and estimated uncertainties in peak extraction and in the assumed background. For the states at higher excitation the total systematic error depends on the correctness of the assumptions used. In the case of the states at 16.7, 18.5, and 20.5 MeV in ${}^5\text{He}$ the error estimates are based on the assumption, discussed earlier, that these are the only states present above the smooth background.

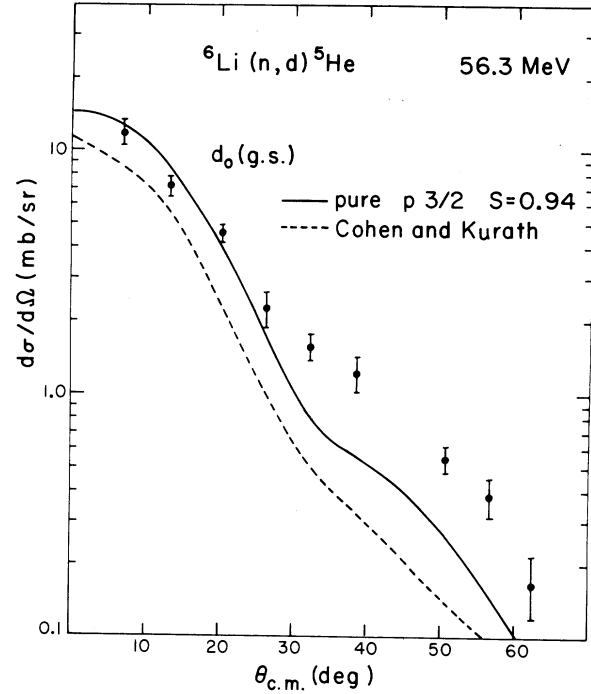


FIG. 4. Angular distribution of ${}^6\text{Li}(n,d){}^5\text{He}$ to the ground state of ${}^5\text{He}$. The solid line is a DWBA fit for the $(p_{3/2})^2$ ${}^6\text{Li}$ g.s. and $S=0.94$. The dashed line uses the spectroscopic factors of Cohen and Kurath.

IV. CALCULATIONS

A. ${}^6\text{Li}(n,d){}^5\text{He}$

Distorted-wave-born-approximation (DWBA) calculations were carried out for proton pickup in the ${}^6\text{Li}(n,d){}^5\text{He}$ reactions using the DWBA program DWUCK4 of Kunz.²⁵

In this mass region, there are two sets of nuclear optical potentials which can be used to generate the distorted waves for nucleons. Mani, Jacques, and Dix²⁶ determined optical potential parameters to describe the elastic scattering of 50 MeV protons on ${}^6\text{Li}$, ${}^7\text{Li}$, and ${}^9\text{Be}$. Since these parameters are expected to vary slowly with mass number and energy, one could use these ${}^6\text{Li}$ optical potential parameters to determine the neutron and proton distorted waves at 56 MeV.

A second set of proton optical model parameters has been determined by Kull¹ in his study of (p,d) reactions on ${}^6\text{Li}$, ${}^7\text{Li}$, and ${}^9\text{Be}$. Kull also gives the optical model parameters for deuterons on ${}^7\text{Li}$ and ${}^9\text{Be}$. Since Kull's ${}^6\text{Li}$ optical model parameters gave the best fit to the ${}^6\text{Li}(n,d){}^5\text{He}$ data, his potentials will be used below.

1. ${}^6\text{Li}(n,d_0){}^5\text{He}$

In the ${}^6\text{Li}(n,d_0){}^5\text{He}$ reaction which leaves the residual nucleus ${}^5\text{He}$ in the ground state, one ex-

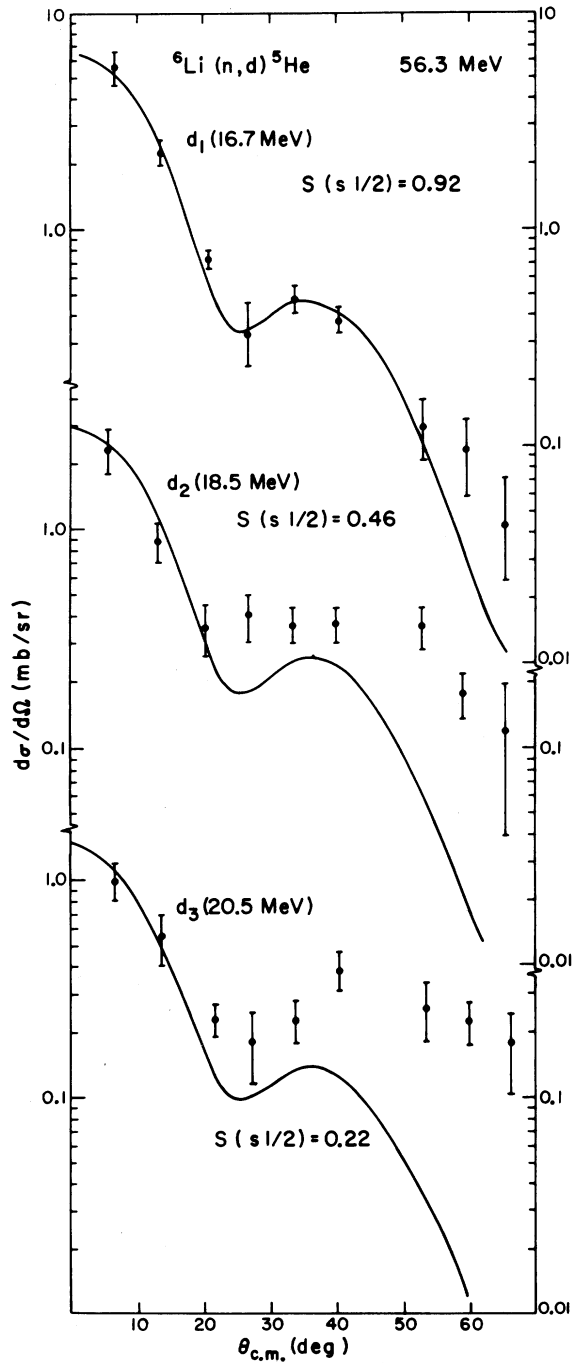


FIG. 5. Angular distributions of ${}^6\text{Li}(n,d){}^5\text{He}$ to excited states of ${}^5\text{He}$ and DWBA predictions assuming $1s_{1/2}$ pickup.

pects to pick up a $1p$ proton. Shell model calculations (e.g., those of Cohen and Kurath²⁷) indicate that both $1p_{3/2}$ and $1p_{1/2}$ orbitals are present in the ground state of ${}^6\text{Li}$. Therefore, the differential cross section will be an incoherent sum of the

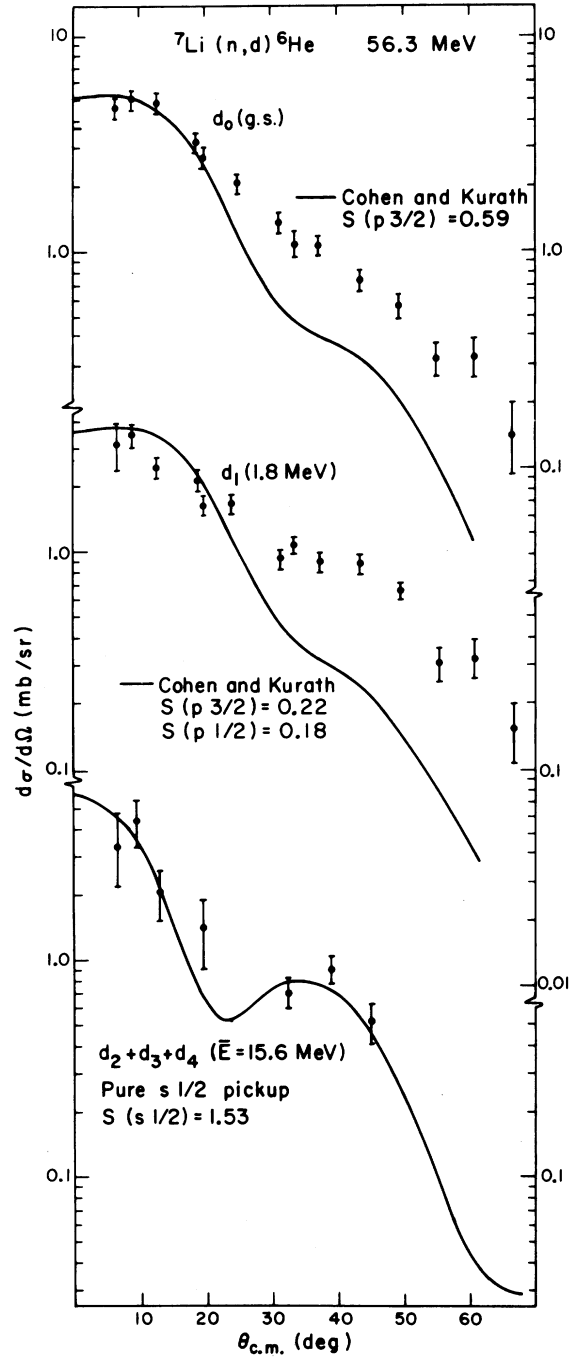


FIG. 6. Angular distributions of ${}^7\text{Li}(n,d){}^6\text{He}$ to states at 0.0 and 1.8 MeV and a group of states centered at 15.6 MeV. The DWBA predictions for d_0 and d_1 used Cohen and Kurath's spectroscopic factors.

cross sections for $1p_{3/2}$ pickup and $1p_{1/2}$ pickup.

The separation energy for a $1p_{3/2}$ particle is 4.59 MeV, so a real Woods-Saxon potential with a Fermi-Thomas spin-orbit term was used which binds the $1p_{3/2}$ particle at -4.59 MeV. The depth

of this Woods-Saxon well was found to be $V_0 = -63$ MeV with $r_0 = 1.25$ fm and $a = 0.65$ fm.

The above well will not bind a $1p_{1/2}$ particle. The $1p_{3/2}$ to $1p_{1/2}$ spin-orbit splitting in this region is about 2.6 MeV.^{27,28} So the $1p_{1/2}$ particle was assumed to be bound by -2.00 MeV and the Woods-Saxon well which gave a binding energy of -2.00 MeV had $V_0 = -75$ MeV with $r_0 = 1.25$ fm and $a = 0.65$ fm.

In order to compare the results of DWUCK4 with the experimental data, and hence determine the spectroscopic factors $S(lj)$, one must know the transferred orbital angular momentum l and the total transferred angular momentum j . In this case the change in parity is given by $(-1)^l$ which implies the pickup of a $1p$ particle since the ${}^6\text{Li}$ and the ${}^5\text{He}$ ground states have opposite parity. The spectroscopic factor $S(lj)$ used in this paper is $8(lj)$ defined by Cohen and Kurath²⁷ times the square of the isotopic-spin Clebsch-Gordan coefficient ($T_f, N_f, \frac{1}{2} - \frac{1}{2} | T_i N_i \rangle^2$ where T_i, N_i, T_f , and N_f refer to the isotopic spin and z component of the target and residual nuclei, respectively. Cohen and Kurath²⁷ (CK) give spectroscopic factors of $S(1p_{3/2}) = 0.32$ and $S(1p_{1/2}) = 0.34$ for this reaction. In Fig. 4, the prediction for the cross section for the ${}^6\text{Li}(n, d_0){}^5\text{He}$ using CK's spectroscopic factors with the results of DWUCK4 is given by the dashed line. The shape is reasonable but the magnitude is too small by $\approx 30\%$. The prediction based on the ${}^6\text{Li}$ wave function of Donnelly and Walecka²⁸ falls just below ($\approx 10\%$) the solid curve of Fig. 4.

If the ground state of ${}^6\text{Li}$ was a pure $(1p_{3/2})^2$ configuration, only $1p_{3/2}$ pickup would be possible. In this case, one can determine the spectroscopic factor $S(1p_{3/2})$ for pure $1p_{3/2}$ pickup from the ratio of σ_{EXP} to σ_{DWUCK4} . The differential cross section for pure $1p_{3/2}$ pickup is the solid curve in Fig. 4 adjusted to fit the forward peak. The spectroscopic factor is determined to be 0.94 which is close to the value of unity which would be predicted by a pure $(1p_{3/2})^2$ configuration for the ground state of ${}^6\text{Li}$.

If the ground state of ${}^6\text{Li}$ was a pure $1p_{3/2}1p_{1/2}$ configuration, only $1p_{1/2}$ pickup would be possible. The curve for $1p_{1/2}$ pickup is similar to the solid line in Fig. 4 except it deviates slightly more from the experimental data at larger angles. The spectroscopic factor determined for pure $1p_{1/2}$ pickup is 0.86 and again is smaller than but close to 1, which would be the case for a pure $1p_{3/2}1p_{1/2}$ configuration for the ${}^6\text{Li}$ ground state.

2. ${}^6\text{Li}(n,d){}^5\text{He}$ to states at 16.7, 18.5, and 20.5 MeV

The energy spectra show peaks at 16.7 and near 18.5 and 20.5 MeV. These states are expected to

have positive parity and to consist mainly of two basic types of configurations. The ground state of ${}^5\text{He}$ is expected to be described by a $(1s_{1/2})^4 1p_{3/2}$ configuration. The positive parity states around 20 MeV are expected to consist of $(1s_{1/2})^3 (1p)^2$ and $(1s_{1/2})^4 (2s1d)$ configurations. The $(1p)^2$ denotes two particles in the $1p$ shell and represents a linear combination of $(1p_{3/2})^2$, $1p_{3/2}1p_{1/2}$, and $(1p_{1/2})^2$ configurations. $(2s1d)$ represents a particle in the $2s1d$ shell. Shell model calculations using these configurations have been done for ${}^6\text{He}$ and they do find several positive parity states in the 15–30 MeV region.^{29,30}

We assume here that the ground state of ${}^6\text{Li}$ contains only $(1p)^2$ configurations. In that case one cannot do a regular one-step DWBA analysis leading to the $(1s_{1/2})^4 (2s1d)$ configurations because it would require the "two-step" process of picking up a $1p$ particle and promoting the other $1p$ particle to the $2s1d$ shell. However, the one-step process can pick up a $1s$ particle leaving the $(1p)^2$ configuration undisturbed. Since the $(1p)^2$ configuration in the ${}^6\text{Li}$ ground state is coupled to $J=1$ and $(1s_{1/2})^3$ has $J=\frac{1}{2}$, these two configurations can only couple to a total J of $\frac{1}{2}$ or $\frac{3}{2}$. On this basis only two states are predicted instead of the three observed. But in ${}^5\text{He}$ one expects the $(1s_{1/2})^3 (1p)^2$ and $(1s_{1/2})^4 (2s1d)$ configurations to mix causing the $(1s_{1/2})^3 (1p)^2$ strength to be distributed over several levels and not just two. Indeed, this configuration mixing appears to be verified experimentally as described below.

Using Kull's optical model parameters,¹ cross sections were calculated with DWUCK4 for pure $1s_{1/2}$ pickup from ${}^6\text{Li}$. The $1s_{1/2}$ radial wave function was computed by using the same Woods-Saxon well which bound the $1p_{3/2}$ particle at -4.59 MeV. The $1s_{1/2}$ binding energy was found to be -22.2 MeV which compares favorably with other estimates of the $1s_{1/2}$ binding energy in this region.

The results of these calculations for the three observed excited states of ${}^5\text{He}$ at 16.7, 18.5, and 20.5 MeV are shown in Fig. 5 where the calculated curves have been adjusted to give the "best fit" to the experimental data at forward angles. It is seen that the (n, d_1) experimental data are fairly well described. The (n, d_2) and (n, d_3) calculated cross sections fall below the experimental data at the large angles even though the forward peak is fairly well reproduced. This may be an indication of the presence of other states of higher angular momentum which are reached via $l=2$.

From the ratios of the experimental to DWUCK4 cross sections, the spectroscopic factors for pure $1s_{1/2}$ pickup were determined to be 0.92, 0.46, and 0.22 for the states at 16.7, 18.5, and 20.5, respectively. The sum of these three spectroscopic factors is

1.60 which is to be compared with the maximum value of 2 expected for the case where all the $1s_{1/2}$ strength is observed. These results verify that the $1s_{1/2}$ strength has been distributed over at least three and probably more states by configuration mixing as described above.

A calculation of the spectroscopic factors for the ${}^6\text{Li}(n, d){}^5\text{He}$ reaction was made as follows. One assumes that the ${}^6\text{Li}$ ground state is given by

$$|{}^6\text{Li}1^+, 0\rangle = a_1 |p_{3/2}{}^2 1^+, 0\rangle + a_2 |p_{3/2} p_{1/2} 1^+, 0\rangle + a_3 |p_{1/2}{}^2 1^+, 0\rangle.$$

Other possible configurations would require at least $2\hbar\omega$ of excitation energy and are expected to have very small amplitudes. The values of a_i from the spectroscopic factor calculations of Cohen and Kurath (CK)²⁷ and from Donnelly and Walecka (DW)²⁸ are given in Table III (top part).

With a $1s_{1/2}$ pickup from the assumed ${}^6\text{Li}(\text{g.s.})$, the ${}^6\text{Li}(n, d){}^5\text{He}$ reaction can only go the $\frac{1}{2}^+$ and $\frac{3}{2}^+$ levels of ${}^5\text{He}$. These excited states in ${}^5\text{He}$ can be written as

$$|{}^5\text{He}JT\rangle = b_1 |\bar{s}_{1/2}(p_{3/2}{}^2 1, 0)JT\rangle + b_2 |\bar{s}_{1/2}(p_{3/2} p_{1/2} 1, 0)JT\rangle + b_3 |\bar{s}_{1/2}(p_{1/2}{}^2 1, 0)JT\rangle + \text{other},$$

where $\bar{s}_{1/2}$ represents a $1s_{1/2}$ hole and the "other" represents additional configurations in the wave function which cannot be connected to the ${}^6\text{Li}$ ground state via a "one-step" pickup reaction. The amplitudes b_i are given in Table III (bottom) for the three lowest levels of each spin.³⁰

The spectroscopic factors $S(lj)$ calculated from the

ground state wave functions of ${}^6\text{Li}$ and the ${}^5\text{He}$ excited states as discussed above are given in Table IV. In terms of the amplitude coefficients a_i and b_i the spectroscopic factors are given by

$$S(lj) = (2J_f + 1) \left(\sum_i a_i b_i \right)^2 / 3,$$

where the only nonzero terms in the sum are the product of coefficients which can have the same $(1p^2)1^+0$ configuration in each wave function. Calculations for the ${}^6\text{Li}$ wave functions of both CK and DW are given in Table IV and may be compared with experimental values of $S(lj)$ obtained via DWBA calculations. The agreement is fairly good for the 16.7 and 20.5 MeV states, but not for the 18.5 MeV state.

B. ${}^7\text{Li}(n, d){}^6\text{He}$

In the ${}^7\text{Li}(n, d){}^6\text{He}$ reactions, states are observed at 0.0 and 1.8 MeV excitation in ${}^6\text{He}$ and a group of states between about 13 and 18 MeV excitation. There is evidence in the energy spectra that at least three states centered near 13.6, 15.4, and 17.7 MeV are present which have the correct kinematic variation with angle (see Fig 3). However, due to poor resolution, limited statistical accuracy, and possibly the energy width of these states and others which may be present, it is not possible to be at all certain of these states. Thus, the data in this region of excitation energy were combined as a single broad peak centered at 15.6 MeV.

TABLE III. Amplitude coefficients used in the calculation of $S(lj)$ to the excited states of ${}^5\text{He}$ for $1s_{1/2}$ proton pickup from ${}^6\text{Li}$ (g.s.).

${}^6\text{Li}$	Reference	Calc. energy (Exper. energy)	Level J^π, T	a_1	a_2	a_3
${}^5\text{He}$	CK ^a	g.s.	$1^+, 0$	0.564	-0.820	0.091
	DW ^b	g.s.	$1^+, 0$	0.810	-0.581	0.084
				b_1	b_2	b_3
	WW ^c	17.7 (16.7)	$\frac{3}{2}^+, \frac{1}{2}$	0.330	-0.660	0.020
	WW ^c	19.6 (18.5)	$\frac{1}{2}^+, \frac{1}{2}$	0.238	-0.410	0.131
	WW ^c	21.9 (20.5)	$\frac{3}{2}^+, \frac{1}{2}$	0.186	-0.345	0.006
	WW ^c	26.2	$\frac{3}{2}^+, \frac{1}{2}$	-0.490	0.317	0.105
	WW ^c	27.1	$\frac{1}{2}^+, \frac{1}{2}$	-0.443	0.258	0.704
	WW ^c	28.6	$\frac{1}{2}^+, \frac{1}{2}$	0.252	-0.446	0.631

^aReference 27.

^bReference 28.

^cReference 30.

TABLE IV. Comparison of experimental and theoretical spectroscopic factors. The experimental values are given assuming pure $1p_{3/2}$, $1p_{1/2}$, or $1s_{1/2}$ pickup.

Residual nucleus	Exper. energy (Calc. energy)	J^π (Calc.)	Experimental $S(lj)$			Theoretical $S(lj)$	
			$1p_{3/2}$	$1p_{1/2}$	$1s_{1/2}$	CK + WW	DW + WW
${}^5\text{He}$	g.s.	$\frac{3}{2}^-$	0.94	0.86		0.65	0.82
	16.7 (17.7)	$(\frac{3}{2}^+)$			0.92	0.71	0.57
	18.5 (19.6)	$(\frac{1}{2}^+)$			0.46	0.15	0.13
	20.5 (21.9)	$(\frac{3}{2}^+)$			0.22	0.20	0.17
${}^6\text{He}$	g.s.	0^+	0.62			0.59	0.56 ^a 0.57 ^b
	1.8	2^+	0.37	0.32		0.40	0.34 ^a 0.41 ^b
	15.6 group	$(1^+, 2^+)$			1.53		

^aReference 31.^bReference 32.1. ${}^7\text{Li}(n,d_0){}^6\text{He}$

The ${}^7\text{Li}(n,d_0){}^6\text{He}$ reaction is a $(\frac{3}{2}^-, \frac{1}{2}) \rightarrow (0^+, 1)$ transition. Parity and angular momentum considerations dictate that only $1p_{3/2}$ pickup is possible. A real Woods-Saxon potential with a Fermi-Thomas spin-orbit term was adjusted to bind the $1p_{3/2}$ particle at -9.98 MeV which is the $1p_{3/2}$ separation energy. The parameters of the Woods-Saxon well were $V_0 = -68.5$ MeV, $r_0 = 1.25$ fm, and $a = 0.65$ fm.

Cohen and Kurath²⁷ give a spectroscopic factor of $S(1p_{3/2}) = 0.59$ for this reaction. Using this spectroscopic factor and DWUCK4, the differential cross section was calculated and is plotted with the experimental data points in Fig. 6(a) (top). It is seen that the Cohen and Kurath spectroscopic factor gives a very good fit to the forward peak. A best fit to the five most forward data points assuming pure $1p_{3/2}$ pickup yields $S(1p_{3/2}) = 0.62$, in good agreement with the CK value of 0.59.

2. ${}^7\text{Li}(n,d_1){}^6\text{He}$

The ${}^7\text{Li}(n,d_1){}^6\text{He}$ reaction is a $(\frac{3}{2}^-, \frac{1}{2}) \rightarrow (2^+, 1)$ transition and can have contributions from pickup of both $1p_{3/2}$ and $1p_{1/2}$ particles. The $1p_{3/2}$ particle was bound at -9.98 MeV in the same Woods-Saxon well described above. The $1p_{1/2}$ particle was bound at -7.38 MeV (a spin-orbit splitting of 2.60 MeV) by a Woods-Saxon well with $V_0 = -81.4$ MeV, $r_0 = 1.25$ fm, and $a = 0.65$ fm.

Using the Cohen and Kurath spectroscopic factors of $S(1p_{3/2}) = 0.217$ and $S(1p_{1/2}) = 0.182$ and DWUCK4, the differential cross section was calculated as an incoherent sum of $1p_{3/2}$ and $1p_{1/2}$ pickup and is compared with the experimental cross section in Fig. 6(b) (middle). (Actually, the j dependence of the

calculations is small.) Although the calculated cross section is a little higher than the data at forward angles, they agree fairly well. The calculated cross section falls off much faster than the data at larger angles. Fitting the data with DWBA predictions yields $S(1p_{3/2}) = 0.37$ for pure $1p_{3/2}$ pickup and $S(1p_{1/2}) = 0.32$ for pure $1p_{1/2}$ pickup. Since the j dependence of the DWBA calculations is small, these spectroscopic factors may be compared with the sum of the CK values which is 0.40.

3. ${}^7\text{Li}(n,d_2 + d_3 + d_4){}^6\text{He}$

As described above, the group of states in the range 13 to 18 MeV was combined together with an average energy of 15.6 MeV. As with the (n,d_1) , (n,d_2) , and (n,d_3) reactions on ${}^6\text{Li}$, it is expected that these higher excitations result from a $1s_{1/2}$ pickup from the ${}^7\text{Li}$ core. The $1s_{1/2}$ wave function was found to have a binding energy of -28.5 MeV using the same Woods-Saxon well described above which bound the $1p_{3/2}$ particle at -9.98 MeV.

DWUCK4 was used to calculate the differential cross section for a pure $1s_{1/2}$ pickup and is compared with the experimental data in Fig. 6(c) (bottom). It is seen that the shape of the differential cross section is fairly well reproduced. The corresponding spectroscopic factor is $S(1s_{1/2}) = 1.53$. Since the maximum $S(1s_{1/2})$ is 2, this result indicates that some of the $1s_{1/2}$ spectroscopic strength probably resides in higher-lying states resulting from configuration mixing as in the ${}^6\text{Li}(n,d){}^5\text{He}$ case.

V. SUMMARY

The ${}^6\text{Li}(n,d){}^5\text{He}$ and ${}^7\text{Li}(n,d){}^6\text{He}$ reactions have been measured using a 56.3 MeV neutron beam with

an energy resolution of ≈ 1 MeV FWHM. Transitions to the ground state ($1p$ -shell pickup) and to a group of states at high excitation in ${}^5\text{He}$ are strong. The latter are interpreted as $1s$ -shell pickup. In this group, there is evidence for states centered near 18.5 and 20.5 MeV, besides that for the well-established 16.7 MeV state. In the case of ${}^7\text{Li}(n, d){}^6\text{He}$, transitions to the states at 0.0 and 1.8 MeV corresponding to $1p$ -shell pickup are strong. The transitions to a group of states centered at 15.6 MeV excitation are also strong and presumably correspond mainly to $1s$ -shell pickup. There is rather inconclusive evidence that these states at high excitation in ${}^6\text{He}$ include (at least) three states centered at energies near 13.6, 15.4, and 17.7 MeV. There is also some evidence (Fig. 3) for a state or states near 23.7 MeV in ${}^6\text{He}$ which appears to require an l transfer ≥ 2 .

Table IV summarizes the experimental and theoretical spectroscopic factors including the spectroscopic factors based on calculations of Barker³¹ (given by Kull¹) and of Balashov, Boyarkina, and Rotter.³² The values given under CK are the sum where allowed of the $1p_{1/2}$ and $1p_{3/2}$ values of CK.²⁷ The uncertainties in the experimental values are difficult to estimate. The uncertainties in the measurements discussed in Sec. III must be combined with the uncertainties in the DWBA calculations. The latter include both uncertainties in the DWBA theory using (corrected) zero range and in the parameters used in the DWBA calculations.

In general, the absolute spectroscopic factors inferred from the present experimental measure-

ments are in fairly good agreement with those obtained from calculations as described above in Sec. IV. For transitions to the ground state of ${}^5\text{He}$, the spectroscopic factors calculated by CK²⁷ and DW²⁸ are a bit smaller ($\approx 30\%$ and $\approx 10\%$, respectively) than the experimental values. For the group of excited states in ${}^5\text{He}$, the sum of the experimental spectroscopic factors is 1.60. This can be compared with a maximum value of 2 expected for $1s_{1/2}$ strength, or with the calculations of Sec. IV which predict the sum of $S(lj)$'s to the three lowest $\frac{1}{2}^+$ and three lowest $\frac{3}{2}^+ 1s_{1/2}$ hole states to be 1.75 in the case where CK²⁷ wave functions are used for ${}^6\text{Li}$ (g.s.), and 1.61 in the case where those of DW²⁸ are used.

For the ${}^7\text{Li}(n, d){}^6\text{He}$ reaction the experimental spectroscopic factor is in good agreement with the theoretical value for the ground state transition and about 10% smaller than theoretical for the first excited state. In the case of transitions to the group of states centered at 15.6 MeV, $S(1s_{1/2})$ is determined experimentally to be 1.53, indicating that further strength probably resides in higher-lying and/or broader states.

ACKNOWLEDGMENTS

We thank Mike Bollen and Rick Spielman for their considerable help in target preparation and in data analysis. We are also indebted to Bill Cline and Jim Harrison for considerable and willing help with hardware and software whenever it was needed and to Gene Russell and crew for the reliable beams.

*Supported in part by the National Science Foundation Grant No. PHY71-03400.

†Present address: Los Alamos Scientific Laboratory, Los Alamos, New Mexico 87544.

‡Present address: LAMPF Visitors Center, Los Alamos, New Mexico 87544.

§Present address: Naval Surface Weapons Center, Maryland 20910.

¹L. A. Kull, Phys. Rev. **163**, 1066 (1967).

²J. K. P. Lee, S. K. Mark, P. M. Portner, and R. B. Moore, Nucl. Phys. **A106**, 357 (1967).

³T. Y. Li and S. K. Mark, Nucl. Phys. **A123**, 147 (1969).

⁴D. Bachelier, M. Bernas, I. Brissand, C. Détraz, and P. Radvanzt, Nucl. Phys. **A126**, 60 (1969); I. S. Towner, *ibid.* **A126**, 97 (1969).

⁵J. G. Likely, Phys. Rev. **98**, A1536 (1955).

⁶J. B. Reynolds and K. G. Standing, Phys. Rev. **101**, 158 (1956).

⁷E. F. Bennett and D. R. Maxson, Phys. Rev. **116**, 131 (1959).

⁸T. H. Short and N. M. Hintz, Bull. Am. Phys. Soc. **9**, 391 (1964); University of Minnesota Linac Laboratory Progress Report No. 61, 1964 (unpublished).

⁹W. Selove, Phys. Rev. **101**, 231 (1956).

¹⁰V. Valkovic, G. Paic, I. Slaus, P. Tomas, and M. Cerineo, Phys. Rev. **139**, B331 (1965).

¹¹D. Miljanic, M. Furic, and V. Valkovic, Nucl. Phys. **A148**, 312 (1970); D. Miljanic and V. Valkovic, *ibid.* **A176**, 110 (1971).

¹²R. H. Lindsay, W. Toems, and V. Veit, Nucl. Phys. **A199**, 513 (1973).

¹³D. F. Measday, Phys. Lett. **21**, 62 (1966); D. F. Measday and J. N. Palmieri, Phys. Rev. **161**, 1071 (1967).

¹⁴J. A. Jungerman and F. P. Brady, Nucl. Instrum. Methods **89**, 167 (1970).

¹⁵F. P. Brady, N. S. P. King, M. W. McNaughton, J. F. Harrison, and B. E. Bonner, in *Proceedings of the Conference on Nuclear Cross Sections and Technology, Washington, D. C., 3-7 March, 1975* (NBS Special Publication No. 425, 1975), Vol. I, p. 103.

¹⁶T. A. Cahill (private communication).

¹⁷F. Ajzenberg-Selove and T. Lauritsen, Nucl. Phys. **A227**, 1 (1974) and references therein.

¹⁸P. A. Treado, J. M. Lambert, R. J. Kane, L. A. Beach, E. L. Peterson, and R. B. Theus, Phys. Rev.

- C 7, 1742 (1973).
- ¹⁹J. C. Roynette, M. Arditi, J. C. Jockmart, F. Maxloulou, M. Riou, and C. Ruhla, Nucl. Phys. A95, 545 (1967).
- ²⁰H. W. Baer, J. A. Bistirlich, K. M. Crowe, N. deBotton, J. A. Helland, and P. Truöl, Phys. Rev. C 8, 2029 (1973).
- ²¹R. K. Bhowmik, C. C. Chang, J.-P. Didelez, and H. D. Holmgren, Phys. Rev. C 13, 2105 (1976).
- ²²J.-P. Didelez, C. C. Chang, R. Bhowmik, H. D. Holmgren, R. I. Steinberg, and J. Wu, Bull. Am. Phys. Soc. 19, 1022 (1974).
- ²³T. C. Montgomery, F. P. Brady, B. E. Bonner, W. B. Broste, and M. W. McNaughton, Phys. Rev. Lett. 31, 640 (1973).
- ²⁴J. Binstock, Phys. Rev. C 10, 19 (1974).
- ²⁵P. D. Kunz (private communication).
- ²⁶G. S. Mani, D. Jacques, and A. D. B. Dix, Nucl. Phys. A165, 145 (1971).
- ²⁷S. Cohen and D. Kurath, Nucl. Phys. A101, 1 (1967).
- ²⁸T. W. Donnelly and J. D. Walecka, Phys. Lett. 44B, 330 (1973).
- ²⁹K. Ramavataram and S. Ramavataram, Nucl. Phys. A147, 293 (1970).
- ³⁰R. F. Wagner and C. Werntz, Phys. Rev. C 4, 1 (1971); and (private communication).
- ³¹F. C. Barker, Nucl. Phys. 83, 418 (1966).
- ³²V. V. Balashov, A. N. Boyarkina, and I. Rotter, Nucl. Phys. 59, 417 (1965).